Translating reproducible phase-separated texture in manganites into reproducible two-state low-field magnetoresistance: An imaging and transport study

C. Israel,[1] L. Granja,[2] T. M. Chuang,[3,†] L. E. Hueso,[1,‡] D. Sánchez,[1] J. L. Prieto,[1,§] P. Levy,[2] A. de Lozanne,[3] and N. D. Mathur[1,*]

[1]*Department of Materials Science, University of Cambridge, Pembroke Street, Cambridge CB2 3QZ, United Kingdom*

[2]*Departamento de Física, Comisión Nacional de Energía Atómica, General Paz 1499 (1650) San Martín, Buenos Aires, Argentina*

[3]*Department of Physics, University of Texas, Austin, Texas 78712, USA*

(Received 18 December 2007; revised manuscript received 11 June 2008; published 7 August 2008)

In thin-film $La_{0.6}Ca_{0.4}MnO_3$, conducting-tip and magnetic force microscopy reveal a pattern of nanoscale phase separation that is reproducible across cooling runs. This pattern represents the intersection of buried three-dimensional filamentary ferromagnetic metallic pathways with the sample surface. As an interlayer in current-perpendicular-to-the-plane trilayer devices, this phase-separated material magnetically decouples ferromagnetic metallic $La_{0.7}Ca_{0.3}MnO_3$ electrodes which switch sharply. This yields sharp two-state low-field magnetoresistance that is *also* reproducible across cooling runs. The reproducibility and the magnitude of the resistance jump are linked to highly resistive ($\sim 10^{-12}$ Ω m^2) constrained domain walls in the pathways of the phase-separated interlayer. Phase separation is normally associated with high-field colossal magnetoresistance and, therefore, its exploitation here to produce low-field effects is unusual.

DOI: 10.1103/PhysRevB.78.054409 PACS number(s): 75.47.Lx, 73.43.Qt, 75.60.Ch, 81.16.Rf

The manganites rose to prominence in the 1990s with the discovery[1] of colossal magnetoresistance (CMR), i.e., large changes in electrical resistance driven by large magnetic fields. Interest persists for two reasons. First, the ferromagnetic metallic (FMM) phase is attractive for spintronics[2] because the conduction-electron-spin polarization[3,4] approaches 100 % and is therefore much higher than the values recorded for common magnetic metals such as cobalt (Ref. 5) ~40 %. Second, manganites of appropriate composition display complex magnetic and electronic phase-separation phenomena over a wide range of length scales.[6,7] Here, using epitaxial thin films, we investigate and exploit both the spin-polarized FMM phase and phase separation.

High-field magnetoresistance[1,8,9] (MR) in chemically single-phase manganites is circumstantially[2] associated with magnetic and electronic phase separation.[6,7] Phase separation strongly influences MR effects, but phase separation is not a prerequisite for MR effects, which could (in principle) arise via the interconversion of very different homogeneous phases. In practice, phase separation arises near first-order phase transitions due to nucleation and pinning by imperfections and is associated with pronounced MR effects showing either large high-field jumps,[8,9] e.g., 10^{10} %, or continuous responses.[1] Continuous MR responses, such as the prototypical CMR effect,[1] are so large ($\sim 10^5$ % at 6 T) that even a small applied magnetic field H produces a substantial MR (~50 % at 10 mT). Therefore, low-field memory effects arising due to phase separation can be large and subtle.[10]

Low-field MR in manganites has not hitherto been associated with phase separation. Large low-field effects arise when H serves to align and misalign magnetic domains on either side of grain boundaries,[11] tunnel barriers,[12,13] and nanoconstrictions.[14–16] Small low-field effects in nominally single-domain unpatterned continuous crystals[17] are a manifestation of the high-field CMR effect; when the magnetization switches to align with H, the local magnetic order is enhanced and the resistivity ρ drops sharply.

Unlike in the bulk, thin-film $La_{0.6}Ca_{0.4}MnO_3$ lies at the edge of the FMM phase field.[18] Its FMM volume fraction (<50 %) is therefore smaller than it is in the bulk[19] (where it approaches 100 %) but no microscopic details of the apparent phase coexistence have been published. Here we reveal percolating FMM pathways in a phase-separated 55 nm $La_{0.6}Ca_{0.4}MnO_3$ film using scanning probe techniques. Next, we demonstrate how to exploit this phase separation in $La_{0.7}Ca_{0.3}MnO_3/La_{0.6}Ca_{0.4}MnO_3/La_{0.7}Ca_{0.3}MnO_3$ devices, where the phase-separated interlayer represents a weak magnetic link that decouples the FMM $La_{0.7}Ca_{0.3}MnO_3$ electrodes [cf. magnetic tunnel junctions[12,13] and giant MR (GMR) multilayers]. Current-perpendicular-to-the-plane (CPP) MR measurements yield two distinct states of resistance. We associate the high-resistance state with constrained domain walls in the FMM pathways of the interlayer.

The 55 nm $La_{0.6}Ca_{0.4}MnO_3$ film was grown by pulsed laser deposition (λ=248 nm, 1 Hz, 2.0 J/cm^2, 800 °C, 15 Pa of flowing O_2, and target-substrate distance=8 cm) from a stoichiometric target (Praxair) on polished $10\times5\times0.5$ mm^3 $NdGaO_3$ (001) substrates (orthorhombic *Pbnm*) and annealed *in situ* (~50 kPa O_2, 750 °C, and 1.5 h) before cooling (10 °C/min) to room temperature (RT). Trilayer growth was similar (except the target-substrate distance was 6.5 cm, the anneal was 1 h at 800 °C, and the cooling was uncontrolled). CPP devices (bottom electrode parallel to [100]) were fabricated from trilayers with *in situ* Au metallization (2.5 J/cm^2, RT, base pressure $\sim 10^{-4}$ Pa, and target-substrate distance=6.5 cm) via a procedure previously used[13] for magnetic tunnel junctions (optical lithography, Ar ion milling, and sputtered SiO_2 and Au). Layer thicknesses were determined from film fringes in ω-2θ x-ray scans about $NdGaO_3$ (004) taken with a Philips X'Pert high-resolution diffractometer (λ=1.54 Å, Ge monochromator).

A variable-temperature scanning probe microscope constructed in house[20] was used to acquire the 77 K conducting-tip atomic force microscopy (CAFM) (Ti-Pt coated tips, lat-

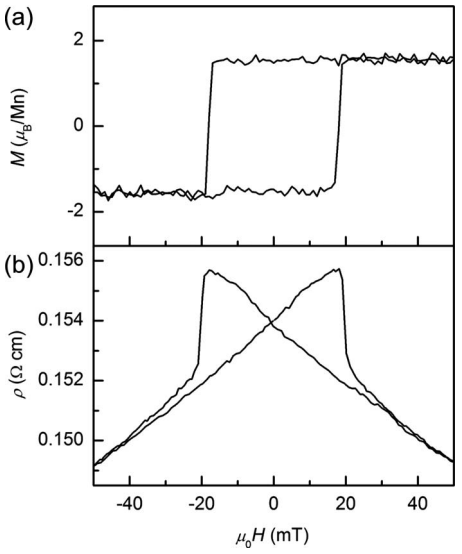

FIG. 1. Magnetic and electrical properties of an unpatterned 55 nm $La_{0.6}Ca_{0.4}MnO_3$ film. (a) Magnetization M at 48 K, and (b) resistivity ρ at 78 K versus H applied along [100].

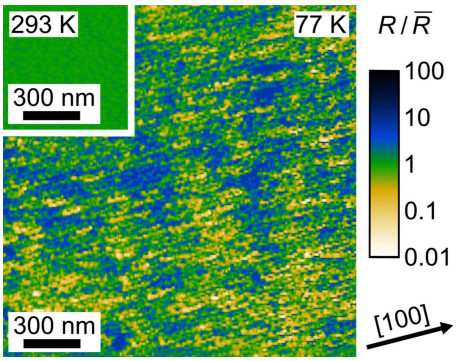

FIG. 2. (Color online) Conducting-tip atomic force microscopy (CAFM) images of the 55 nm $La_{0.6}Ca_{0.4}MnO_3$ film. Two-point resistance R measurements between the conductive nanoscale tip and a biased electrical contact located remotely on the film surface were normalized by the median value $\bar{R}$ for each image. The main image was taken below T_p at 77 K ($\bar{R}$=6 MΩ) and the inset was taken above T_p at 293 K ($\bar{R}$=25 kΩ). When the sample is macroscopically metallic below T_p, the electronic structure exhibits phase separation on a range of length scales.

eral resolution ~10 nm) and magnetic force microscopy (MFM) (Co-Cr coated tips, lateral resolution ~100 nm) images. The 293 K CAFM image was acquired with a Digital Instruments MultiMode atomic force microscope (AFM). Magnetic measurements were performed using a Princeton Measurements Corporation vibrating sample magnetometer and the paramagnetic substrate contribution was removed via a linear fit at high field. Four-terminal resistivity measurements of the film were performed at 50 μA in a continuous-flow cryostat with current and applied field along [100]. Four-terminal CPP device measurements were performed at 100 μA in a He closed-cycle cryostat with the applied field along [100]. Current-voltage characteristics were linear up to 150 μA at all measurement temperatures (20–300 K) and fields (±0.5 T). All transport measurements and magnetometry of films and devices were performed after zero-field cooling and the subsequent application of an applied field that was large enough to remove magnetic domains. This applied field was not unduly large in order to minimize the possibility of irreversible FMM phase-fraction enlargement.[10]

Magnetometry of a 55 nm $La_{0.6}Ca_{0.4}MnO_3$ film [Fig. 1(a)] records a small low-temperature FMM volume fraction (~42 %) and a suppressed Curie temperature T_C (~150 K) as expected.[18] We confirm an in-plane uniaxial easy axis[21] along [100] but note that for films of such extreme composition, the anisotropy can vary with deposition run.[22] The film is insulating at RT and becomes metallic on cooling through T_p=145 K≈T_C. At 78 K, $\rho(H)$ shows sharp drops near the coercive field [Fig. 1(b)] due to magnetization reversal and CMR as discussed earlier. At other fields, $\rho(H)$ is linear and $|d\rho/dH|$=64 % T^{-1} is larger than the corresponding value of 2 % T^{-1} for homogenous FMM $La_{0.67}Ca_{0.33}MnO_3$ films[23] due to the influence of H on FMM volume fraction.

CAFM images of the 55 nm $La_{0.6}Ca_{0.4}MnO_3$ film taken below T_p, in the macroscopically metallic state, reveal a phase separation into electrically conducting and insulating regions. Conducting regions that percolate and reach the film surface appear bright in the CAFM image shown in Fig. 2, where the contrast represents the current that flows between the scanned tip and a biased electrode on the film surface. Isolated conducting regions cannot be detected by this method since they are not connected to the percolated conducting network; their apparent existence in Fig. 2 demonstrates that some percolating pathways pass underneath the film surface, i.e., the phase separation is three dimensional. The in-plane length scale for phase separation is seen to range from 30 nm, which is comparable with the film thickness, up to several hundred nanometers. The unexpected in-plane elongations along [100] could be due to stress arising from the asymmetry of the epitaxial mismatch between $La_{0.6}Ca_{0.4}MnO_3$ (a/b=1.002) and $NdGaO_3$ (b/a=1.013). A CAFM image taken at RT>T_p (inset of Fig. 2) shows drastically reduced variations in contrast implying that the film is electrically homogeneous. Therefore, the low-temperature electronic structure may (in principle) be reset by an excursion to RT.

MFM images of the 55 nm $La_{0.6}Ca_{0.4}MnO_3$ film at 77 K reveal a magnetic phase separation that is reproducible between cooling runs. Figure 3(a) was recorded after zero-field cooling from RT. The magnetic contrast here reveals the presence of a ferromagnetic domain structure but does not in itself confirm the existence of phase separation. Figure 3(b) was recorded after subsequently applying 36 mT along [100] and removing it. This procedure aligns the magnetizations of all ferromagnetic regions since 36 mT is sufficient to saturate the magnetic hysteresis loop and this loop is square [Fig. 1(a)]. Therefore, the persistence of MFM contrast in Fig. 3(b) is attributed to regions of uniformly magnetized ferromagnetic material coexisting with regions of nonferromagnetic material, i.e., phase separation. Indeed, no such contrast is observed in MFM images of magnetized homogeneous FMM films of $La_{0.7}Ca_{0.3}MnO_3$ on $NdGaO_3$, which also have very square magnetic hysteresis loops.[21]

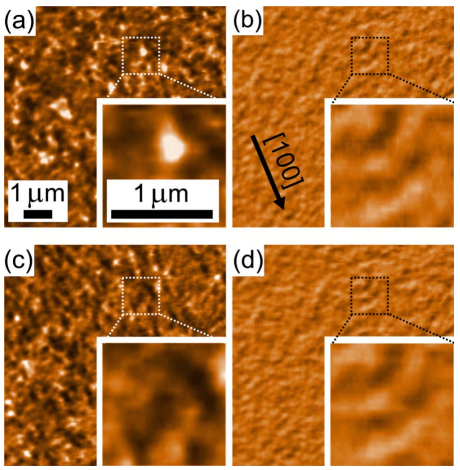

FIG. 3. (Color online) Magnetic force microscopy (MFM) images of a single 8×8 μm^2 area of the same 55 nm $La_{0.6}Ca_{0.4}MnO_3$ film studied in Fig. 2. All images are displayed on an identical contrast scale. Images (a)–(d) show zero-field data at 77 K after different magnetic and thermal histories. After cooling from RT in $H=0$, the magnetic contrast in (a) is significantly reduced by the application and removal of a saturating field of 36 mT along [100] prior to the collection of image (b). Images (c) and (d) correspond to a repeat of this run. The insets, all from a single 1.2×1.2 μm^2 area, show more clearly that the magnetic structure is subject to strong run-to-run variations after cooling in $H=0$, (a), (c) but is recovered with remarkable reproducibility by the application of the field (b), (d).

A repeat zero-field cooling run for exactly the same area of the film generated Figs. 3(c) and 3(d). It is particularly apparent from the insets that the images taken after cooling

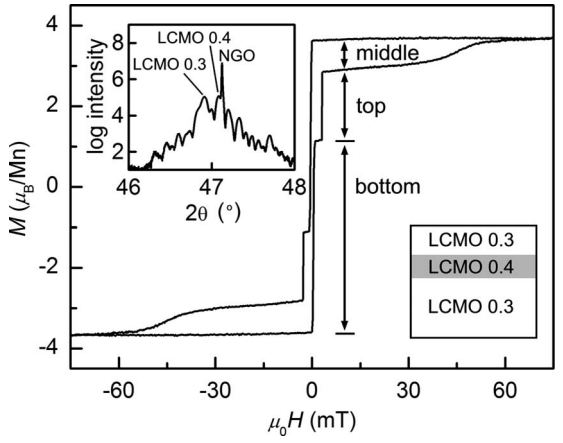

FIG. 4. Magnetic measurements of an unpatterned $La_{0.7}Ca_{0.3}MnO_3$(29 nm)/$La_{0.6}Ca_{0.4}MnO_3$(29 nm)/$La_{0.7}Ca_{0.3}MnO_3$ (72 nm) trilayer. $M(H)$ along [100] at 79 K shows two abrupt jumps associated with top (2.9 ± 0.2 mT) and bottom (0.44 ± 0.10 mT) layer switching. The more diffuse switching in 35–60 mT is due to the FMM regions of the $La_{0.6}Ca_{0.4}MnO_3$ interlayer. Upper inset: ω-2θ x-ray scan about $NdGaO_3$ (004) taken with a Philips X'Pert high-resolution diffractometer ($\lambda=1.54$ Å, Ge monochromator). The observation of peaks for each component of the trilayer confirms the epitaxy of the heterostructure. Lower inset: Trilayer schematic ($La_{1-x}Ca_xMnO_3$ is denoted LCMO x for clarity).

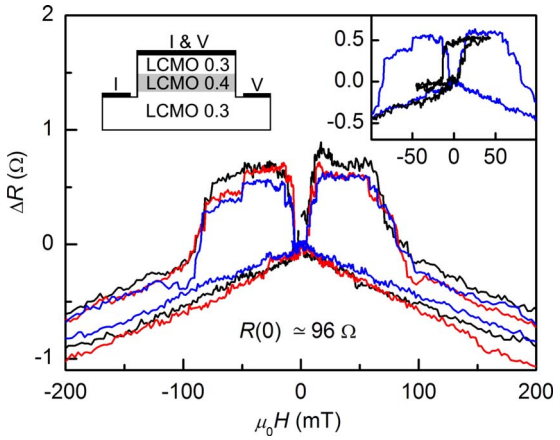

FIG. 5. (Color online) CPP electrical measurements after zero-field cooling to 25 K of a 5×5 μm^2 mesa device patterned from a $La_{0.7}Ca_{0.3}MnO_3$(20 nm)/$La_{0.6}Ca_{0.4}MnO_3$(20 nm)/$La_{0.7}Ca_{0.3}MnO_3$(50 nm) trilayer in which all layers are macroscopically metallic at the measurement temperature. The schematic shows contact pads (thick lines) and voltage V and current I terminals. Each of the three $R(H)$ sweeps was measured after an excursion to RT and we plot $\Delta R=R(H)-R(0)$ to eliminate small extrinsic run-to-run variations in top contact resistance attributed to microstructural changes and other aging effects. For the three sweeps, $R(0)=97.9$ Ω (black), 96.2 Ω (red), and 95.8 Ω (blue). The switching (jump magnitude and switching fields) is highly reproducible from run to run and two distinct states are seen at $H=0$ (minor loop, inset). The upper switching field corresponds to the top electrode (see main text).

[Figs. 3(a) and 3(c)] are very different but become very similar [Figs. 3(b) and 3(d)] after exposure to the magnetic field. This similarity demonstrates that the pattern of phase separation is fixed, e.g., due to fixed local variations in strain.[24–26] This interpretation suggests that the differences between Figs. 3(a) and 3(c) arise due to different magnetic domain configurations in a fixed pattern of ferromagnetic regions.

The insets of Figs. 3(b) and 3(d) reveal a modulation along [100] on a length scale of several hundred nanometers. This is consistent with the longest length scale seen by CAFM (Fig. 2) suggesting a common origin. The finer CAFM features obtained in contact mode cannot be resolved in the MFM images, where the lateral resolution is poorer due to, e.g., tip-sample separation (40 nm), finite tip volume, and divergent fields.

Magnetic measurements of an unpatterned $La_{0.7}Ca_{0.3}MnO_3$(29 nm)/$La_{0.6}Ca_{0.4}MnO_3$ (29 nm)/$La_{0.7}Ca_{0.3}MnO_3$ (72 nm) trilayer (Fig. 4) confirm[22] that the phase-separated interlayer (Figs. 2 and 3) decouples the magnetizations of the two outer FMM layers. CPP trilayer devices (left inset of Fig. 5) therefore permit the exploitation of this phase separation and its run-to-run persistence. At low temperatures, the resistance R of a typical 5×5 μm^2 mesa CPP trilayer device is metallic and $R(H)$ displays two-state switching (Fig. 5). Equivalent results with mesas up to 19×19 μm^2 confirm that the upper switching field is associated with the top electrode. Milling-induced defects[27] are likely to be responsible for both the increase in switching fields and the decrease in switching quality relative to the

unpatterned trilayer (Fig. 4). Assuming the interlayer to be unaffected by milling because it is essentially buried, the fields associated with interlayer reversal in the CPP device fall between the upper and lower switching fields. This guarantees that the resistance state of the device is determined by the magnetic configuration of the $La_{0.7}Ca_{0.3}MnO_3$ electrodes; in the parallel electrode configuration, the interlayer magnetization is aligned with the electrode magnetizations, magnetic domain walls are absent, and R is low; in the antiparallel electrode configuration, R is high due to the formation of magnetic domain walls associated with the FMM pathways of the phase-separated interlayer. These domain walls could span the FMM pathways or they could be extremely sharp as discussed later.

The two distinct states of resistance in Fig. 5 represent an improvement over our recent MR measurements[22] of a similar[18] trilayer that was top contacted in the current-in-the-plane (CIP) geometry. Because this trilayer was unpatterned, the top and bottom layer magnetizations both switched at smaller fields than those associated with interlayer reversal, cf. Fig. 4. Therefore, the transition from the high-resistance state to the low-resistance state with increasing $|H|$ was governed by the magnetic reversal of the interlayer and, hence, it was quasicontinuous rather than sharp. An additional advantage of the CPP geometry employed here is that the current pathways through the interlayer are better defined, which permits the following quantitative analysis.

To establish the low-temperature domain-wall resistance-area (RA) product for the CPP device, we compare R with and without domain walls at $H=0$ via minor loops (right inset of Fig. 5). In order to normalize the measured value of $\Delta R=0.6\ \Omega$, we assume that the relevant cross-sectional area of FMM pathways in the interlayer is 20 %–42 % of the area of the mesa. The upper bound assumes that the 42 % FMM volume fraction—determined by magnetometry—represents the appropriate areal fraction. The lower bound, which recognizes that not all FMM regions are necessarily part of the percolating network, is calculated from the CAFM image (Fig. 2) assuming a cutoff of $R/\bar{R}<0.4$. These bounds yield a small range $3\times10^{-12}\ \Omega\ m^2 \leq RA \leq 6.3\times10^{-12}\ \Omega\ m^2$ that lies within the spread of values recorded for manganite films (i) with patterned and therefore potentially damaged constrictions [$8\times10^{-14}\ \Omega\ m^2$ in $La_{0.7}Ca_{0.3}MnO_3$ (Ref. 14), $1.4\times10^{-11}\ \Omega\ m^2$ in $La_{0.7}Sr_{0.3}MnO_3$ (Ref. 15), and $2.5\times10^{-13}\ \Omega\ m^2$ in $La_{2/3}Sr_{1/3}MnO_3$ (Ref. 16)], and (ii) without constrictions [$1\times10^{-15}\ \Omega\ m^2$ in $La_{0.7}Sr_{0.3}MnO_3$ (Ref. 28)].

The large values of RA seen in manganites exceed the values for standard magnetic metals such as cobalt[29] ($\sim10^{-19}\ \Omega\ m^2$) by more than six orders of magnitude. This could be due to the formation of mesoscopic magnetic and electronic structure at wall centers where the stability of the FMM phase is reduced.[7,14] Indeed, mesoscopic structure is common in the manganites[30] but its possible existence here could not be revealed by current-voltage characteristics because top contact resistance dominates. The large RA could also be due to geometric constraints[31] since (i) the domain walls lie in filamentary FMM pathways (Fig. 1) and (ii) the interlayer is thinner than the natural domain-wall width[32] of 38 ± 10 nm suggested for FMM phases of $(La,Ca)MnO_3$.

In summary, we have demonstrated reproducible two-state low-field MR in CPP manganite trilayer devices, where FMM electrodes ($La_{0.7}Ca_{0.3}MnO_3$) sandwich a phase-separated interlayer ($La_{0.6}Ca_{0.4}MnO_3$) associated with resistive domain walls ($RA\sim10^{-12}\ \Omega\ m^2$). CAFM reveals that thin films of the interlayer material possess filamentary conducting pathways and MFM reveals a fixed pattern of phase separation. We suggest that frozen-in local strain[24–26] fixes the pattern of phase separation and underpins the reproducible device performance.

In the future, the deterministic control of local strain could be exploited to define electrical circuits without[33] the need for top-down or bottom-up fabrication. This approach, which is reminiscent of information storage in rewritable CDs and DVDs, is attractive for miniaturization because it permits the definition of lateral nanoscale features such as our phase-separated FMM pathways without incurring process-related damage.

We thank M. Bibes and H. Y. Hwang for the discussions, L. Fraigi *et al.* at INTI for the technical support, and J. T. Markert (Department of Physics, University of Texas) for the use of his AFM. This work was funded by the EU FP6 STRP CoMePhS (C.I.), the EU Alban Program (L.G.), the ANPCYT PICT under Grant No. 03-13517 (L.G. and P.L.), the U.S. National Science Foundation under Grant No. DMR-0308575 (T.M.C and A.dL.), the Welch Foundation under Grant No. F-1533 (T.M.C and A. dL.), the EU Marie Curie scheme (L.E.H., D.S., and J.L.P.), and the U.K. EPSRC.

*ndm12@cam.ac.uk

†Present address: National High Magnetic Field Laboratory, Florida State University, Tallahassee, Florida 32310, USA.

‡Present address: School of Physics and Astronomy, University of Leeds, Leeds LS2 9JT, UK.

§Present address: Intituto de Sistemas Optoelectrónicos y Microtecnología (ISOM), Universidad Politécnica de Madrid (UPM), Avda. Complutense s/n, Madrid 28040, Spain.

[1] S. Jin, T. H. Tiefel, M. McCormack, R. A. Fastnacht, R. Ramesh, and L. H. Chen, Science **264**, 413 (1994).

[2] C. Israel, M. J. Calderon, and N. D. Mathur, Mater. Today **10**, 24 (2007).

[3] J.-H. Park, E. Vescovo, H.-J. Kim, C. Kwon, R. Ramesh, and T. Venkatesan, Nature (London) **392**, 794 (1998).

[4] M. Bowen, M. Bibes, A. Barthelemy, J. P. Contour, A. Anane, Y. Lemaitre, and A. Fert, Appl. Phys. Lett. **82**, 233 (2003).

[5] R. Meservey and P. M. Tedrow, Phys. Rep. **238**, 173 (1994).

[6] E. Dagotto, *Nanoscale Phase Separation and Colossal Magnetoresistance* (Springer, New York, 2002).

[7] N. D. Mathur and P. B. Littlewood, Solid State Commun. **119**,

271 (2001).
[8] A. Anane, J. P. Renard, L. Reversat, C. Dupas, P. Veillet, M. Viret, L. Pinsard, and A. Revcolevschi, Phys. Rev. B **59**, 77 (1999).
[9] R. Mahendiran, A. Maignan, S. Hebert, C. Martin, M. Hervieu, B. Raveau, J. F. Mitchell, and P. Schiffer, Phys. Rev. Lett. **89**, 286602 (2002).
[10] P. Levy, F. Parisi, L. Granja, E. Indelicato, and G. Polla, Phys. Rev. Lett. **89**, 137001 (2002).
[11] N. D. Mathur, G. Burnell, S. P. Isaac, T. J. Jackson, B. S. Teo, J. L. MacManusDriscoll, L. F. Cohen, J. E. Evetts, and M. G. Blamire, Nature (London) **387**, 266 (1997).
[12] J. Z. Sun, W. J. Gallagher, P. R. Duncombe, L. Krusin-Elbaum, R. A. Altman, A. Gupta, Y. Lu, G. Q. Gong, and G. Xiao, Appl. Phys. Lett. **69**, 3266 (1996).
[13] M. H. Jo, N. D. Mathur, N. K. Todd, and M. G. Blamire, Phys. Rev. B **61**, R14905 (2000).
[14] N. D. Mathur, P. B. Littlewood, N. K. Todd, S. P. Isaac, B. S. Teo, D. J. Kang, E. J. Tarte, Z. H. Barber, J. E. Evetts, and M. G. Blamire, J. Appl. Phys. **86**, 6287 (1999).
[15] J. Wolfman, A. M. Haghiri-Gosnet, B. Raveau, C. Vieu, E. Cambril, A. Cornette, and H. Launois, J. Appl. Phys. **89**, 6955 (2001).
[16] T. Arnal, A. V. Khvalkovskii, M. Bibes, B. Mercey, P. Lecoeur, and A. M. Haghiri-Gosnet, Phys. Rev. B **75**, 220409(R) (2007).
[17] J. O'Donnell, M. Onellion, M. S. Rzchowski, J. N. Eckstein, and I. Bozovic, Phys. Rev. B **55**, 5873 (1997).
[18] D. Sanchez, L. E. Hueso, L. Granja, P. Levy, and N. D. Mathur, Appl. Phys. Lett. **89**, 142509 (2006).
[19] S.-W. Cheong and H. Y. Hwang, in *Colossal Magnetoresistive Oxides*, edited by Y. Tokura (Gordon and Breach, Amsterdam, 2000).
[20] T.-M. Chuang and A. de Lozanne, Rev. Sci. Instrum. **78**, 053710 (2007).
[21] N. D. Mathur, M. H. Jo, J. E. Evetts, and M. G. Blamire, J. Appl. Phys. **89**, 3388 (2001).
[22] L. E. Hueso, L. Granja, P. Levy, and N. D. Mathur, J. Appl. Phys. **100**, 023903 (2006).
[23] A. Gupta, G. Q. Gong, G. Xiao, P. R. Duncombe, P. Lecoeur, P. Trouilloud, Y. Y. Wang, V. P. Dravid, and J. Z. Sun, Phys. Rev. B **54**, R15629 (1996).
[24] D. D. Sarma *et al.*, Phys. Rev. Lett. **93**, 097202 (2004).
[25] K. H. Ahn, T. Lookman, and A. R. Bishop, Nature (London) **428**, 401 (2004).
[26] Y. A. Soh, G. Aeppli, N. D. Mathur, and M. G. Blamire, Phys. Rev. B **63**, 020402(R) (2000).
[27] M. H. Jo, N. D. Mathur, and M. G. Blamire, Appl. Phys. Lett. **80**, 2722 (2002).
[28] Y. Wu, Y. Suzuki, U. Rudiger, J. Yu, A. D. Kent, T. K. Nath, and C. B. Eom, Appl. Phys. Lett. **75**, 2295 (1999).
[29] U. Rudiger, J. Yu, L. Thomas, S. S. P. Parkin, and A. D. Kent, Phys. Rev. B **59**, 11914 (1999).
[30] N. Mathur and P. Littlewood, Phys. Today **56** (1), 25 (2003).
[31] P. Bruno, Phys. Rev. Lett. **83**, 2425 (1999).
[32] S. J. Lloyd, N. D. Mathur, J. C. Loudon, and P. A. Midgley, Phys. Rev. B **64**, 172407 (2001).
[33] N. Mathur and P. Littlewood, Nat. Mater. **3**, 207 (2004).